Bremsstrahlung of nitrogen and noble gases in single-bubble sonoluminescence

Ning Xu,[1] Long Wang,[1] and Xiwei Hu[2]
[1]*Institute of Physics, Chinese Academy of Sciences, Beijing 100080, People's Republic of China*
[2]*University of Science and Technology of China, Hefei 230026, People's Republic of China*
(Received 12 March 1999; revised manuscript received 15 September 1999)

A hydrodynamic model, discussing neutral gases as well as plasmas, is applied to simulate single-bubble sonoluminescence. In this model, thermal conduction and various inelastic impact processes such as dissociation, ionization, and recombination are considered. Bremsstrahlung is assumed as the mechanism of the picosecond light pulse in sonoluminescence. Diatomic nitrogen and noble gas bubbles are studied. The results show that the sonoluminescing bubbles are completely optically thin for bremsstrahlung. The calculated spectra agree with previous observations, and can explain the observed differences in spectra of different gases.

PACS number(s): 78.60.Mq, 47.40.−x, 34.80.Dp, 51.20.+d

As periodic ultrasonic waves of high intensity focus into a degassed liquid, e.g., water, a bubble will be trapped and emit picosecond flashes of ultraviolet light [1–3]. This phenomenon is known as single-bubble sonoluminescence (SBSL). A single sonoluminescing bubble shows a continuous broad spectrum shaped like the tail of the spectrum of blackbody radiation or bremsstrahlung [4]. The intensity of the light is sensitive to the gas composition in the bubble. Noble gases are able to emit high intensity sonoluminescence (SL), while diatomic gases, e.g., N_2, show very faint emission [5]. Air bubble SL is theoretically attributed to the 1% Ar in the air [6]. The experimental spectra [4] suggest the existence of photons with energy above 6 eV, but unfortunately the water cuts off observation of this possibility.

Several theoretical explanations have been proposed for this unique nonlinear phenomenon [7–15]. A thermal radiation mechanism [7–13] is prevalent among them. Hydrodynamic descriptions were applied in this explanation to simulate the gas motion in a sonoluminescing bubble [7,8]. These simulations described the propagation of the shocks and qualitatively explained some observations. In our previous work [16], we described a hybrid model including the descriptions of neutral gases and plasmas to simulate the processes of Ar bubble SL. In the calculations, the evolution of the plasma in the Ar bubble was carefully studied, and bremsstrahlung was assumed as the mechanism of the SL. Recent experiments [17–19] indicate that the pulse widths and emission times of SL are independent of the light wavelength from ultraviolet to infrared. These observations suggest that SL might originate in a plasma, which may emerge and quench instantaneously due to the violent motion of the bubble wall; the source of the SL would be thermal bremsstrahlung.

In the framework of shock models, some incomprehensible phenomena occurring in SL can be explained further. For example, it is found that an air bubble can emit high intensity SL, while a pure N_2 bubble can hardly emit any light [5], although about 79% of the air is N_2. It has been assumed that the sonoluminescing air bubble might become an Ar bubble after sufficient chemical reactions between N_2 and the surrounding water [6]. Experiments [5] also showed the fact that Ar bubbles are much brighter than N_2 bubbles. Why is there such a remarkable difference in SL intensity between N_2 and Ar bubbles? Due to the difference in the polytropic exponent γ, N_2 should be compressed more strongly than Ar. The temperature in N_2 should also reach a higher maximum. Thus, N_2 bubbles should not be much fainter than Ar bubbles. To explain this puzzle, Moss *et al.* carried out well-known calculations [9] discussing the opacity of the bubbles. They obtained partially optically thick bubbles during the bubbles' final collapse. The spectra were thus calculated on the hypothesis that SL was a convolution of Planckian and bremsstrahlung emission. The opacity of N_2 is two to three times greater than that of Ar, but the radiating volume of N_2 is much smaller than that of Ar. These facts lead to the Ar bubbles being much brighter than N_2 bubbles.

In this paper, we intend to exploit our detailed plasma model to reexamine the question of N_2 vs Ar SL. The results to some extent accord with the work of Moss *et al.*, but the underlying mechanisms are quite different. Furthermore, applying the same model, we study the emission features of different noble gases. There is an observed tendency in noble gas SL that the spectra will shift more to the ultraviolet as the gas inside the bubble changes from Xe to He. How to explain this tendency is a challenge to every theoretical model.

Like most of the previous calculations, we assume spherical symmetry of the bubble and calculate only one cycle of the repetitive oscillations. The motion of the bubble wall is described by the Rayleigh-Plesset (RP) equation [7]. Detailed processes of inelastic impact among the gas particles in the bubble are studied. Because of the high gas density, collisions are frequent and soon the different components reach local thermodynamic equilibrium. Based on this consideration, we assume a well-defined local temperature. Thermal conduction is also included here. The details will be discussed below. Surface tension and viscosity are ignored. The acoustic field is expressed as $P_a(t) = -P_a \sin(\omega_a t)$. The values of P_a have a significant effect on the intensity of the light pulse, as was shown in most of the previous work and will be discussed also in this paper. The acoustic frequency ω_a and the ambient bubble radius R_0 are also critical to the calculations. Their values in the case of our calculations will be listed below. The ambient pressure P_0 and temperature T_0

used here are, respectively, 1 atm and 20 °C. The details stated below are for a pure N_2 bubble. Noble gases can be treated by the same method, without the dissociation processes pertaining to diatomic molecules. The equations of mass, momentum, and energy are

$$\frac{D\rho_i}{Dt}+\rho_i\nabla\cdot\mathbf{v}=m_i\dot{n}_i, \tag{1}$$

$$\rho\frac{D\mathbf{v}}{Dt}=-\nabla(P+Q), \tag{2}$$

$$\rho\frac{DE}{Dt}+(P+Q)\nabla\cdot\mathbf{v}=-\nabla\cdot\mathbf{q}-U_r, \tag{3}$$

$$\rho=\sum\ \rho_i=\sum\ m_i n_i, \tag{4}$$

$$\frac{D}{Dt}=\frac{\partial}{\partial t}+\mathbf{v}\cdot\nabla, \tag{5}$$

where ρ, $\mathbf{v}$, P, Q, E, $\mathbf{q}$, and U_r are, respectively, the density, velocity, pressure, artificial viscosity [20], internal energy, heat flow, and energy loss due to radiation; ρ_i and m_i are the density and mass of different particles such as molecules, atoms, and ions; and $\dot{n}_i$ is the rate of change of the number density n_i due to inelastic collisions. We include degrees of ionization up to 5. The electron density can be obtained from the hypothesis of quasineutrality. Charge separation ought to be considered under the circumstances of shock propagation [21]. We do not include this effect here in order to simplify the problem, because charge separation may not have much influence on the final light output.

For N_2, the inelastic processes considered here are dissociation and recombination. For atoms and ions, electron collisional ionization, radiative recombination, and three-body recombination are included. This description is a better way to obtain more detailed information of the plasma processes in the bubble. There are two main reversible inelastic processes of N_2 [22,23]:

$$\mathrm{N_2+N_2}\overset{1}{\rightleftharpoons}\mathrm{N+N+N_2},$$

$$\mathrm{N+N_2}\overset{2}{\rightleftharpoons}\mathrm{N+N+N}.$$

The processes involving the molecular ion N_2^+ are not under consideration here. The corresponding expressions for $\dot{n}_{N_2}$, $\dot{n}_N(\dot{n}_0)$, and $\dot{n}_j(j=1,2,\ldots,5)$ are then

$$\dot{n}_{N_2}=-(n_{N_2})^2\alpha_{d_1}-n_N n_{N_2}\alpha_{d_2}+(n_N)^2 n_{N_2}\alpha_{r_1}+(n_N)^3\alpha_{r_2}, \tag{6}$$

$$\dot{n}_N=-2\dot{n}_{N_2}-n_N n_e\alpha^{ion}_{0\to1}+n_1 n_e\alpha^{rec}_{1\to0}, \tag{7}$$

$$\dot{n}_j=-n_j n_e(\alpha^{ion}_{j\to j+1}+\alpha^{rec}_{j\to j-1})+n_{j-1}n_e\alpha^{ion}_{j-1\to j}+n_{j+1}n_e\alpha^{rec}_{j+1\to j}, \tag{8}$$

$$\alpha^{rec}_{j\to j-1}=\alpha^{rrec}_{j\to j-1}+\alpha^{trec}_{j\to j-1}, \tag{9}$$

where $\alpha_{d_1}(\alpha_{d_2})$ and $\alpha_{r_1}(\alpha_{r_2})$ are the rates of the forward and reverse reactions of N_2 listed above [22,23], and $\alpha^{ion},\alpha^{rrec}$, and α^{trec} are the rates of ionization, radiative recombination, and three-body recombination [24–26].

Thermal conduction is believed to be one of the main energy losses that contribute to the picosecond pulse width and the absence of the ''afterglow'' which should emerge under the hypothesis of thermal radiation but is not observed in experiments [9]. Under the extreme conditions of SL, the classical Spitzer-Härm (SH) transport may not always be valid. In a steep temperature gradient, the heat flow described by the SH model may exceed the limit of its validity. In order to avoid possibly erroneous calculations, we exploit the heat flow widely used in inertial confinement fusion (ICF) in steep temperature gradients [27]:

$$q=fq_f, \tag{10}$$

where $f<1$ is the flux limit and q_f is the free streaming limit given by [27]

$$q_f=n_e kT_e(kT_e/m_e)^{1/2}, \tag{11}$$

where k is the Boltzmann constant, T_e is the electron temperature, and m_e is the mass of an electron. Because of the uncertainties of SL, we cannot determine the suitable value of f through comparisons between our calculations and experiments (the method used in ICF). We have used values of f in the range from 0.01 to 0.1. The results are not very sensitive to such a change. Thus, we adopt the value 0.03, which is typically used in ICF.

There is not yet an exact equation of state for the unique conditions of SL. The equation of state in Ref. [16] is adopted here, in which dissociation, ionization, and a hard van der Waals core are included. Our calculations have verified its feasibility. The equation of state is

$$P=\frac{\left(n_{N_2}+n_e+\sum_{i=0}^{5}n_i\right)kT}{1-b\rho}, \tag{12}$$

$$E=\frac{1}{\rho}\left(\frac{5}{2}n_{N_2}kT+\frac{3}{2}n_e kT+\frac{3}{2}\sum_{i=0}^{5}n_i kT+E_d+E_I\right), \tag{13}$$

where T, b, E_d, and E_I are, respectively, the temperature, van der Waals excluded volume, dissociation energy, and ionization energy.

In a plasma, bremsstrahlung contributes most of the photons with low energy. The absorption of bremsstrahlung is also considered here in order to avoid missing possible reabsorption. The spectral absorption coefficient κ_ν of bremsstrahlung is [28]

$$\kappa_\nu=\frac{4}{3}\left(\frac{2\pi}{3m_e kT}\right)^{1/2}\frac{Z_i^2 e^6}{hcm_e\nu^3}n_i n_e, \tag{14}$$

where Z_i, e, h, c, and ν are, respectively, the charge number of the ions, the charge of an electron, the Planck

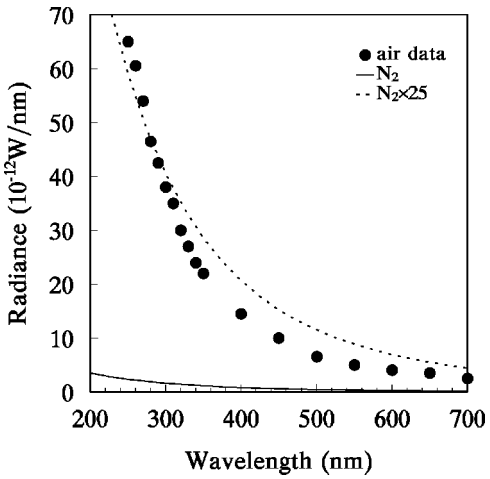

FIG. 1. The calculated spectrum of a pure N_2 bubble. The dots are the air data obtained in experiment [4]. The solid and dotted lines are, respectively, the calculated spectrum and the multiplied one. The pure N_2 bubble is shown to be more than 20 times dimmer than the air bubble.

constant, light speed, and light frequency. For emission between 180 and 750 nm, the total power $\mathcal{P}$ can be expressed as

$$\mathcal{P}=\int_0^R 4\kappa\sigma T^4 \exp\left(-\int_r^R \kappa dr'\right)\pi r^2 dr, \tag{15}$$

where κ is the frequency-averaged absorption coefficient of bremsstrahlung between 180 and 750 nm and σ is the Stefan-Bolzmann constant.

We use a Lagrangian scheme to solve Eqs. (1)–(3) numerically. The combination of all the above equations and the RP equation forms a complete and solvable numerical problem.

Figure 1 shows the calculated spectrum of SL emitted from a pure N_2 bubble with $R_0=4.5$ μm driven by an acoustic pressure $P_a=1.37$ atm. The acoustic frequency ω_a is $2\pi\times 26.5$ kHz. The radiance $\mathcal{R}$ can be calculated by

$$\mathcal{R}(\nu)=\sum_{Z_i}\frac{1}{T_a}\int_0^{T_a}\int_0^R 4\kappa_\nu\sigma T^4 \exp\left(-\int_r^R \kappa_\nu dr'\right)\pi r^2 dr\, dt, \tag{16}$$

where T_a is the period of the acoustic oscillations. The air data obtained in experiment [4] are also listed as a comparison. The calculated data agree well with the fact that a pure N_2 bubble is about 30 times dimmer than an air bubble [5]. Due to the lower γ, the sound speed in N_2 is lower than that in noble gases, and hence much stronger shocks are launched. Our calculation shows a very high peak temperature (more than 1 keV) at such a N_2 bubble's center because of the violent heating. However, high temperatures only emerge in a very thin layer around the bubble center and decrease swiftly. Consequently, a nitrogen plasma layer with very high density exists for a very short time and emits a high power flash. Because of the swift quenching of the nitrogen plasma, this vast output is not long maintained. The existence of the thin and ephemeral plasma layer in a N_2 bubble can be explained as follows. Because N_2 must first undergo dissociation to produce the plasma, to obtain an electron, the combined energy of dissociation and ionization is needed. The strength of the shocks causes very steep temperature gradients near the bubble center. Thus, only in a very thin layer around the bubble center, can the temperature satisfy the conditions for N_2 to produce dense plasma. In contrast with this dense plasma layer, plasma is very rare in the remainder of the bubble. The radiating volume in a N_2 bubble is hence limited to such a layer. Figure 2(a) shows the time evolutions of the bubble radius, output power, and the boundary of the radiating volume from which 99% of the total light is emitted. Although the peak power is above 70 mW, the pulse width is only about 0.2 ps, so the time-integrated radiation is still very low. The peak power occurs about 9 ps before the bubble radius reaches its minimum. The main radiating volume is confined in a sphere with a radius less than $0.2R(t)$, where $R(t)$ is the time-dependent bubble radius.

In order to make some comparisons, we also present the calculated results for sonoluminescing pure Ar bubbles. Figure 2(b) shows the time evolutions of the bubble radius, output power, and the boundary of the radiating volume of a $R_0=4.5$ μm Ar bubble driven by a $P_a=1.4$ atm and $\omega_a=2\pi\times 26.5$ kHz acoustic pressure. As mentioned above, it is harder for an Ar bubble to launch shocks than a N_2 bubble. Under such a driving pressure, shocks in an Ar bubble are weak. The peak temperature hence reaches only about 50 eV. As is shown in Fig. 2(b), the peak power is a little less than 10 mW. However, the radiating volume is much greater than that of the N_2 bubble discussed above. The pulse width is about 42 ps, which is also much wider than that of the N_2 bubble. All these lead to the higher time-integrated radiation, which can be seen from a comparison between Figs. 1 and 3.

It is also known that a bubble will emit more light as the acoustic pressure increases. The reason is simple under the hypothesis of shock-induced emission. As the driving pres-

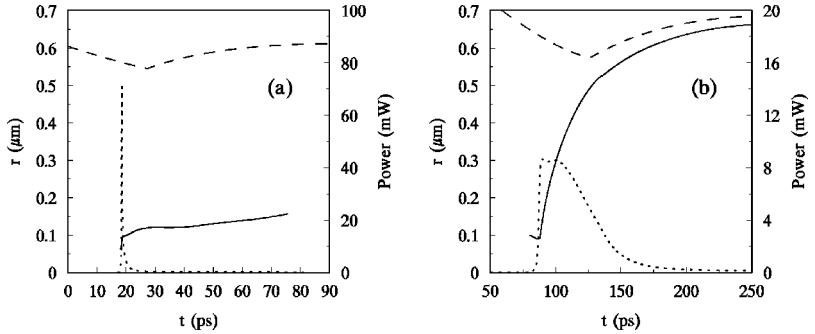

FIG. 2. Time evolutions of the emitting power, bubble radius, and boundary of the emitting regions, shown as dotted line, dashed line, and solid line respectively. (a) A pure N_2 bubble with ambient radius $R_0=4.5$ μm, driven by acoustic pressure $P_a=1.37$ atm. (b) A pure Ar bubble with ambient radius $R_0=4.5$ μm, driven by acoustic pressure $P_a=1.4$ atm. The frequency ω_a is $2\pi\times 26.5$ kHz.The emitting boundary delineates the spheres in which 99% of the total light is emitted.

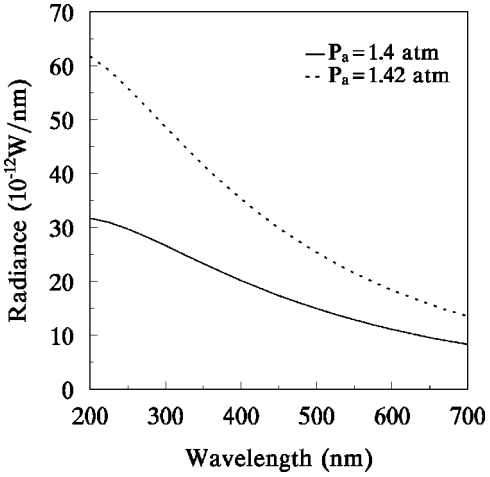

FIG. 3. Calculated spectra of pure Ar bubbles in two cases: $P_a=1.4$ atm and $P_a=1.42$ atm. The ambient radius is 4.5 μm in both cases. The frequency ω_a is $2\pi\times 26.5$ kHz.

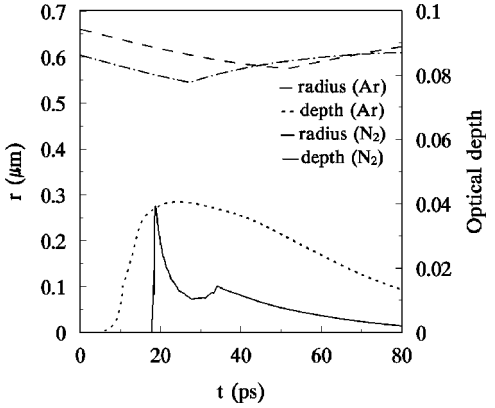

FIG. 4. Time evolutions of optical depth for the two cases in Fig. 2. The optical depth is calculated throughout the whole bubble radius.

sure increases, if R_0 is left unchanged, the bubble will reach a larger maximum radius. Thus, the bubble wall will collapse more violently. The consequence is more violent heating and the generation of a plasma with higher density and temperature. More light will be emitted by bremsstrahlung. The two calculated spectra in Fig. 3 indicate this relation between the driving pressure and the emission. We adopt the same ambient radius in the two cases. Only 0.02 atm increase of the driving pressure causes a twofold output.

In recent studies, Hilgenfeldt *et al.* and Frommhold described their models to calculate the SL spectra [11–13]. Bremsstrahlung was also assumed as the main emission mechanism in their models, and they all included electron-neutral bremmstrahlung. In our calculations, the ionization is relatively stronger than theirs. For example, in the case listed in Fig. 2(b), at the moment just after the shocks reflect from the bubble center, the ionization degree reaches about 0.80 at the bubble center. As the shocks propagate outward, their strength declines, so the ionization degree behind the shock front drops. However, the globally averaged ionization degree with respect to the total bubble is always larger than 0.10 when the emitting power is higher than 20% of its maximum. Therefore, time-integrated electron-neutral bremsstrahlung is much weaker than electron-ion bremsstrahlung and thus the effect of electron-neutral bremsstrahlung is not considered. However, we reach a common conclusion with Hilgenfeldt *et al.* and Frommhold that a sonoluminescing bubble is optically thin, so blackbody radiation should not be the mechanism of SBSL. Figure 4 shows the optical depth of the N_2 and Ar bubbles discussed driven by 1.37 atm and 1.4 atm acoustic pressure, respectively. The optical depth-D_{opt} is dimensionless and is calculated from

$$D_{\mathrm{opt}}=\int_0^R \kappa\, dr. \tag{17}$$

The calculated peak values are no more than 0.1. For an optically thick medium, the optical depth should be more than 1. Therefore, a sonoluminescing bubble is completely optically thin for bremsstrahlung. The light is emitted almost without reabsorption. This result is quite different from Moss *et al.*'s work [9]. However, our calculations still show very similar spectral radiances to theirs. This agrees with the viewpoint that the output of SBSL is mostly contributed by the optically thin region in the bubble. Even in their calculations, the occurrence of the optically thick region does not influence the final output, because it is ephemeral and its volume is very small. Since it is the main emission mechanism in the optically thin region, bremsstrahlung should be the overwhelming source of SBSL.

Noble gas SBSL has been studied experimentally [5,18]. Comparison among different noble gas spectra shows that from Xe to He the spectra are more and more ultraviolet. These experiments also stress that a sonoluminescing Xe bubble shows a maximum in its spectrum near 300 nm. Here, we calculate the spectra of these noble gases. The results reproduce these observations well. Figure 5 shows the calculated spectra of SBSL emitted by different kinds of noble

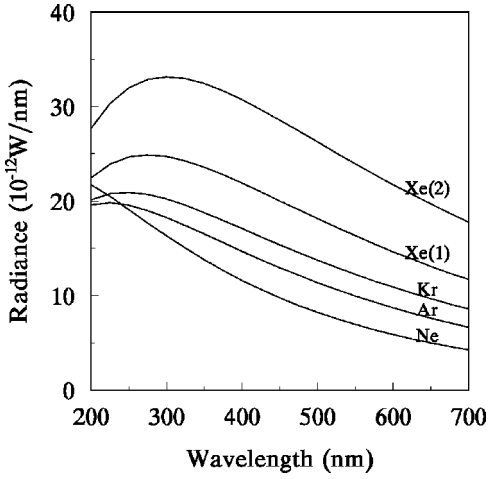

FIG. 5. The calculated spectra of different noble gases. There are two cases calculated for Xe bubble SL [Xe(1) and Xe(2)]: (1) $R_0=5.0$ μm and $P_a=1.37$ atm; (2) $R_0=6.0$ μm and $P_a=1.4$ atm. The ambient radius R_0 of the calculated Kr, Ar, and Ne bubbles is identically 5.0 μm. The acoustic frequency ω_a is $2\pi\times 33$ kHz in all the cases.

gases. The driving frequency ω_a is $2\pi\times 33$ kHz in all the cases. The ambient radius is 5.0 μm in the cases of Ne, Ar, and Kr. Two cases of Xe bubble's are calculated here: (1) $R_0=5.0$ μm and $P_a=1.37$ atm; (2) $R_0=6.0$ μm and $P_a=1.4$ atm. The acoustic pressure is adjusted in the cases of Ne, Ar, and Kr in order to obtain similar SL intensity as in case (1) of the Xe bubble. Our calculations show that, as the filling gas is changed from Xe to Ne, it is harder and harder for the bubble to transit into SL. This tendency is shown by the increase of the needed acoustic pressure from Xe to Ne in the listed cases. It can be seen from Fig. 5 that the spectra are more and more ultraviolet from Xe to Ne. There is also a broad maximum near 300 nm in the spectrum of Xe, especially in case (2). It is easy to understand this tendency by our model. Two main factors, atomic mass and ionization potential, determine it. For noble gases, because the sound speed is in inverse proportion to the square root of the atomic mass (if the number density of the gas is similar), the heavier the atom, the lower the sound speed. Shocks will hence be more easily launched in heavier gases, which leads the bubbles to transit easily into SL. Furthermore, from Ne to Xe, the ionization potential and the temperature needed for ionization are both decreasing. It is easier for a heavier gas to produce plasma. In reverse, the emergence of the plasma will increase the free particle number density and thus decrease the temperature. The rate of recombination for the plasma in a heavier gas is slower due to the low ionization potential. Therefore, it is easier for a heavier noble gas to maintain a high density and low temperature plasma for a relatively longer time. This plasma contributes most of the emission. It is known that the peak of a bremsstrahlung spectrum will shift to a longer wavelength as the temperature drops. From Ne to Xe, the temperatures in which most of the radiation is emitted are decreasing, so the maximum of the spectra will shift to longer wavelength (redshift). The SL of Xe bubbles shown here is typical of such low temperature emissions. The broad maximum in Xe spectra illustrates that low temperature (about 2 eV) emissions predominate in Xe bubble SBSL.

In Fig. 6, the light pulses and the bubble radii of the two discussed cases of Xe are compared. The minimum bubble radii R_{min} in the two cases are about 0.76 and 0.92 μm, respectively, so the ratios $(R_0/R_{min})^3$ are about 284.8 and 277.3, respectively. This means that the bubble in case (1) is compressed more violently than that in case (2). In case (2), shocks propagate a longer distance than in case (1). The direct representation in our calculations is the higher peak temperature at the center of the bubble in case (2). However, if we ''walk'' along the bubble radius toward the center from the bubble wall, we can see that in most parts of the bubble, the temperature in case (2) is lower than that in case (1). This can be seen from Fig. 5: the spectrum of the bigger bubble has a maximum at longer wavelength than that of the smaller one. A bubble with a larger ambient radius contains more gas, which means that more charged particles will participate in radiation. Although the bigger bubble is compressed a little more weakly, the higher driving pressure and larger radiating volume still make the bubble in case (2) brighter than that in case (1) (see Fig. 5). The pulse widths of the two cases are about 126 and 171 ps, respectively. A bigger bubble needs a relatively longer time to be completely cooled down, so the bigger bubble shows a larger pulse width than the smaller one. As the driving acoustic pressure increases, the stable ambient bubble radius may become larger. The comparison of the two cases here may somewhat explain the previous observations that the pulse width increases along with the driving pressure [17].

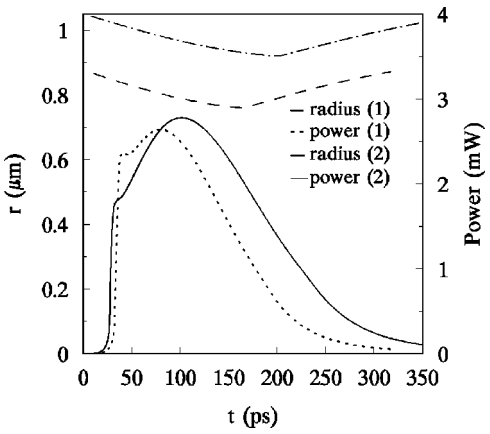

FIG. 6. Time evolutions of the emitting power and bubble radius for the two cases of Xe bubbles shown in Fig. 5.

In conclusion, we have explained two distinguishable phenomena in SBSL by a detailed plasma model: the dim emission of pure N_2 bubbles and differences in the spectra of noble gases. The dim emission of a pure N_2 bubble is due to the higher energy needed for plasma generation and the small radiating volume. In [9], Moss *et al.* stated similar results for pure N_2 SBSL. We here reach the common view with them that the small radiating volume determines the dim emission and the radiating volume is the key to the final light output of SBSL. The tendency to spectral shift among noble gas SL is due to the differences in atomic mass and ionization potential. In addition, the sonoluminescing bubbles are completely optically thin for bremsstrahlung, which has also been shown by Hilgenfeldt *et al.* and Frommhold's calculations. Shocks still occur in our calculations, without taking the effects of neutral gas viscosity and thermal conduction into account. Here, shocks act to compress and ionize gases. The effects on the total emission cannot be neglected. Because many theoretical models can give similar SBSL spectra, the differences among the models might not be easily distinguished by today's experimental methods. However, the agreements between our calculations and experiments suggest that the plasma produced in the bubble during the bubble's violent collapse should be a key factor in understanding SBSL.

This work was supported by NSFC Contract No. 19875052 and 19934001.

[1] D.F. Gaitan and L.A. Crum, J. Acoust. Soc. Am. Suppl. 1 **87**, S141 (1990).
[2] B.P. Barber and S.J. Putterman, Nature (London) **352**, 318 (1991).
[3] B.P. Barber *et al.*, Phys. Rep. **281**, 65 (1997).
[4] R. Hiller, S.J. Putterman, and B.P. Barber, Phys. Rev. Lett. **69**, 1182 (1992).
[5] R. Hiller, K. Weninger, S.J. Putterman, and B.P. Barber, Science **266**, 248 (1994).
[6] D. Lohse *et al.*, Phys. Rev. Lett. **78**, 1359 (1997).
[7] C.C. Wu and P.H. Roberts, Phys. Rev. Lett. **70**, 3424 (1993).
[8] W.C. Moss, D.B. Clarke, J.W. White, and D.A. Young, Phys. Fluids **6**, 2979 (1994).
[9] W.C. Moss, D.B. Clarke, and D.A. Young, Science **276**, 1398 (1997).
[10] L. Frommhold and A.A. Atchley, Phys. Rev. Lett. **73**, 2883 (1994).
[11] S. Hilgenfeldt *et al.*, Nature (London) **398**, 402 (1999).
[12] S. Hilgenfeldt *et al.*, Phys. Fluids **11**, 1318 (1999).
[13] L. Frommhold, Phys. Rev. E **58**, 1899 (1998).
[14] C. Eberlein, Phys. Rev. Lett. **76**, 3842 (1996).
[15] T. Lepoint *et al.*, J. Acoust. Soc. Am. **101**, 2012 (1997).
[16] Ning Xu, Long Wang, and Xiwei Hu, Phys. Rev. E **57**, 1615 (1998).
[17] B. Gompf *et al.*, Phys. Rev. Lett. **79**, 1405 (1997).
[18] R.A. Hiller, S.J. Putterman, and K.R. Weninger, Phys. Rev. Lett. **80**, 1090 (1998).
[19] R. Pecha *et al.*, Phys. Rev. Lett. **81**, 717 (1998).
[20] J. von. Neumann and R.D. Richtmyer, J. Appl. Phys. **21**, 232 (1950).
[21] Ning Xu, Long Wang, and Xiwei Hu, Phys. Rev. Lett. **83**, 2441 (1999).
[22] P. Hammerling, J.D. Teare, and B. Kiwel, Phys. Fluids **2**, 422 (1959).
[23] S. Lin and J.D. Teare, Phys. Fluids **6**, 355 (1963).
[24] D.L. Book, NRL Plasma Formulary, NRL Publication, Washington, D.C., 1987.
[25] D.E. Post *et al.*, At. Data Nucl. Data Tables **20**, 398 (1977).
[26] A. Erdas and P. Quarati, Z. Phys. D: At., Mol. Clusters **28**, 185 (1993).
[27] M. H. Key, *Handbook of Plasma Physics* (Elsevier Science Publishers, Amsterdam, 1991), Vol. 3, Chap 14.
[28] Ya.B. Zel'dovich and Yu.P. Raizer, *Physics of Shock Waves and High-Temperature Hydrodynamic Phenomena* (Academic Press, New York, 1966), Chap 5.